Superstructure of the centromeric complex of TubZRC plasmid partitioning systems

Christopher H. S. Aylett and Jan Löwe[1]

Medical Research Council Laboratory of Molecular Biology, Division of Structural Studies, Cambridge CB2 0QH, United Kingdom

Edited by J. Richard McIntosh, University of Colorado, Boulder, CO, and approved August 30, 2012 (received for review June 26, 2012)

Bacterial plasmid partitioning systems segregate plasmids into each daughter cell. In the well-understood ParMRC plasmid partitioning system, adapter protein ParR binds to centromere *parC*, forming a helix around which the DNA is externally wrapped. This complex stabilizes the growth of a filament of actin-like ParM protein, which pushes the plasmids to the poles. The TubZRC plasmid partitioning system consists of two proteins, tubulin-like TubZ and TubR, and a DNA centromere, *tubC*, which perform analogous roles to those in ParMRC, despite being unrelated in sequence and structure. We have dissected in detail the binding sites that comprise *Bacillus thuringiensis tubC*, visualized the TubRC complex by electron microscopy, and determined a crystal structure of TubR bound to the *tubC* repeat. We show that the TubRC complex takes the form of a flexible DNA–protein filament, formed by lateral coating along the plasmid from *tubC*, the full length of which is required for the successful in vitro stabilization of TubZ filaments. We also show that TubR from *Bacillus megaterium* forms a helical superstructure resembling that of ParR. We suggest that the TubRC DNA–protein filament may bind to, and stabilize, the TubZ filament by forming such a ring-like structure around it. The helical superstructure of this TubRC may indicate convergent evolution between the actin-containing ParMRC and tubulin-containing TubZRC systems.

FtsZ | X-ray crystallography | DNA segregation

Low copy number plasmids often encode their own segregation machinery, ensuring that copies are partitioned into each daughter cell. These plasmid-partitioning systems organize replicated plasmids and actively separate them. The known plasmid-partitioning systems are minimalist and elegant. They consist of just three components: a DNA centromere, an adapter protein that binds the centromere, forming the centromeric complex, and a nucleotide triphosphate-dependent filament-forming protein, which produces the force to move the plasmids (1, 2).

Plasmid partitioning systems have been divided into types I–III, based upon the homology of their filament-forming proteins to known protein families (2, 3). Type I plasmid partitioning systems (4, 5) are based on deviant Walker A ATPases (6, 7), type II (8) on actin-like proteins (9), and type III (10–12) on tubulin/FtsZ-like proteins (13, 14). Although the structure of the filament implicated in segregation has been determined for all three systems (9, 14–16), only examples of type I and II centromeric complexes have so far been resolved (17–19).

The centromeric complex of the type II (actin-like) ParMR*C* plasmid partitioning system is formed by the binding of adapter protein ParR to *parC*, a series of parallel (direct), 11-base pair (bp) repeats (20). The superstructure this complex forms is helical, right-handed, and places the *parC* DNA on the exterior of the helix and ParR on the interior (18, 19). This arrangement clusters the interaction surfaces between ParM and ParR, which are located at the tip of the ParM filament and within the last few residues of ParR (18, 19). This clustering probably enables processive filament tip tracking by promoting binding between the filament end and the R*C* helix, ensuring that only *parC*-bound ParR is able to seed and grow, or at least stabilize filaments.

The centromeric complex of the type III (tubulin-like) TubZR*C* plasmid partitioning system is also composed of an adapter, TubR, and a DNA centromere, *tubC*. The rough disposition of four of the repeats making up *Bacillus thuringiensis* serovar *israelensis* pBtoxis (*Bt*) *tubC*, but not the TubR binding site or register, has been assigned by Tang and colleagues who demonstrated binding by *Bt* TubR to this region of pBtoxis (10, 21). Furthermore, the structure of the TubR adapter protein has been determined in the absence of DNA (13), revealing that it forms a recognition-helix dimer with a potential DNA binding surface and demonstrating that it is unrelated to type II ParR (18, 19). Finally, it has been shown that the TubR*C* complex is capable of recruiting TubZ (13, 21). A summary of previous work on the TubZRC system is provided in Table S1.

In this study we examine in detail the superstructures formed by TubR*C* complexes. We show that *Bt tubC* in fact contains seven high-affinity binding sites, the full region being required for proper in vitro activity. Furthermore we reveal that TubR coats *tubC*: the centromeric complex of TubZR*C* plasmid partitioning systems therefore takes the form of a DNA–protein filament. We present a 7.0-Å crystal structure revealing the superstructure of the flexible *Bt* TubR*C* filament and provide electron microscopy and a 3.5-Å crystal structure that imply a preferred conformation for the TubR*C* filament of *Bacillus megaterium* (*Bm*), allowing us to compare the superstructures of type III (tubulin-like) centromeric complexes to those of type II (actin-like) plasmid partitioning systems.

Results

***Bt tubC* Dissected by Microarray.** We initially set out to precisely define *B. thuringiensis* (*Bt*) *tubC*. The structure of the centromere is defined by the binding of its protein partner; therefore, we dissected the binding of *Bt* TubR to each independent site within this part of pBtoxis. We designed a microarray in which each experimental measurement consisted of a 24-bp double-stranded DNA sequence (Fig. 1*B*), formed by a hairpin stabilized through a tetraloop (22). This 24-base "window" was scanned through the plasmid in successive measurements; a 4-bp shift per measurement was used to conduct a coarse scan of a large area of pBtoxis, and single base pair shifts were then used for a high-resolution scan of the *Bt tubC* region (Fig. 1 *B* and *C*). *Bt* TubR bound the array in only a few places, and binding was sustained reproducibly with the movement of the experimental window. The *Bt tubC* region was readily identified as the sole site of strong, sustained binding.

***Bt* TubR Binds to *tubC* Cooperatively.** Peaks of binding by *Bt* TubR were clearly identifiable (Fig. 1*C*). Fourier analysis of this signal with respect to sequence confirmed the repeat length to be between 12 and 13 bp (Fig. S1) (10). We aligned the sequences producing peak signal allowing for a 12-bp repeat and produced a weighted consensus sequence of the repeats found in *Bt tubC* (Figs. S1 and S2). Two directly repeated sequences were required to produce each peak, troughs in binding occurring

Author contributions: C.H.S.A. and J.L. designed research; C.H.S.A. performed research; C.H.S.A. and J.L. analyzed data; and C.H.S.A. and J.L. wrote the paper.

The authors declare no conflict of interest.

This article is a PNAS Direct Submission.

Data deposition: The atomic coordinates and structure factors have been deposited in the Protein Data Bank, www.pdb.org (PDB ID codes 4ASN, 4ASO, and 4ASS).

[1]To whom correspondence should be addressed. E-mail: jyl@mrc-lmb.cam.ac.uk.

This article contains supporting information online at www.pnas.org/lookup/suppl/doi:10.1073/pnas.1210899109/-/DCSupplemental.

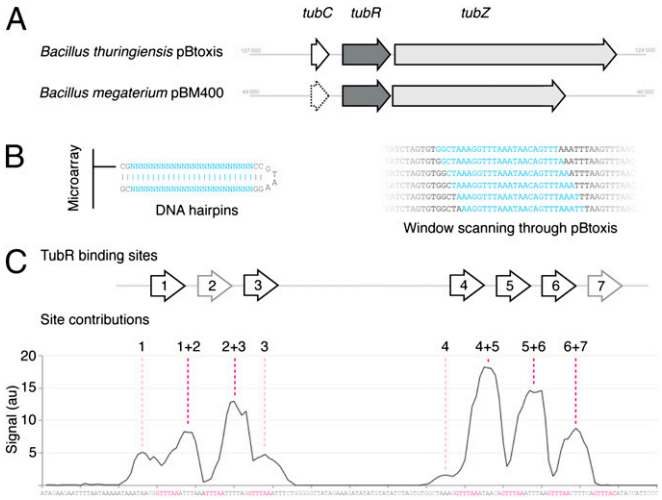

Fig. 1. *Bt tubC* is composed of seven repeats, which bind TubR in a cooperative fashion. (*A*) Schematic comparing the *tubZRC* loci of *Bt* pBtoxis and *Bm* pBM400. (*B*) Illustration of the DNA hairpins produced on a microarray to sample the sequence of pBtoxis, and a schematic indicating how this window was scanned through a region of the plasmid sequence by successive single base pair movements. The variable window is shown in cyan, and all other base pairs in black. (*C*) Plot of the recorded signal for each microarray spot in a 1-bp scan over the region of *Bt tubC* (bp 126688 to 126496). Each point is plotted over the 12th bp of the 24-bp hairpin, with the sequence shown below. The assigned binding sites for *Bt* TubR are shown above, and the corresponding sequences are colored magenta below. The site(s) resulting in each peak have been annotated above the graph.

on centering of a single binding site (Fig. 1*C* and Fig. S2), implying that *Bt* TubR binding is highly cooperative, dependent on lateral stabilization. This mechanism is consistent with the known activity of TubR as a repressor (12), providing a mechanism by which affinity may be tuned. Stronger sites (such as sites 1, 3, and 4) were capable of supporting binding on adjacent DNA, indicated by low signal peaks in the absence of adjacent cognate sites, implying that spreading of *Bt* TubR along the plasmid is possible (Fig. 1*C*). We confirmed that such lateral spreading occurs in vitro by electrophoretic mobility shift assay (Fig. S3).

***Bt tubC* Is Seven TubR Binding Sites in Two Clusters.** *Bt* TubR binding was limited almost exclusively to the region of DNA 3′ from *tubR*. Whereas four direct repeats have previously been identified (21) we found that there are in fact two clusters of *Bt* TubR binding sites, the first comprising three adjacent sites (sites 1–3) and the second four (sites 4–7), which together we identify as the native *Bt tubC* (Fig. 1*C*). Each block binds *Bt* TubR independently in vitro (Fig. S3). Because the two blocks are separated by 54 bp, spreading of *Bt* TubR cannot coat all intervening DNA; however, it is well established in the case of ParR from *Escherichia coli* plasmid R1 that separate blocks of sites are linked by looping of the intervening DNA, so a single complex may be formed (18, 23). Evolution has selected for the production of an array of *Bt tubC*-bound TubR dimers; these must presumably therefore be required to perform the function of the TubR*C* centromeric complex.

***Bt* TubR*C* Forms a DNA–Protein Filament in Vitro.** To understand why *Bt tubC* had evolved an array of parallel repeats, we examined the complex formed by *Bt* TubR on its centromere using electron microscopy. We produced full-length, untagged *Bt* TubR and purified it to homogeneity (Fig. 2*A*); it was then bound to a PCR product encompassing the full *Bt tubC* region. DNA–protein filaments composed of blocky subunits were clearly visible in samples of the *Bt* TubR*C* complex (Fig. 2*B*). *Bt* TubR*C* filaments had an average width measuring 5–6 nm, consistent with the greatest width of a single TubR dimer, whereas the separation of the subunits (from Fourier transform) was 4–5 nm, suggesting that a single fiber of *Bt tubC* DNA was bound by a single row of TubR dimers. The filaments were typically extended, although some exhibited a higher degree of curvature, indicating that these complexes are flexible.

Structure of *Bt* TubR*C* at 7 Å. Unfortunately the *Bt* TubR*C* DNA–protein filaments were not sufficiently ordered for either helical or single-particle reconstruction; therefore, we obtained a higher resolution model by cocrystallizing *Bt* TubR with oligonucleotides from *tubC*. Cocrystals were obtained with *Bt* TubR and a 24-bp double-stranded oligonucleotide (*tubC*24). Diffraction was recorded to 7 Å. The structure shown in Fig. 2 *C*–*E* was solved by molecular replacement using PDB ID code 3M9A and B-form DNA (13) and verified by phasing selenium anomalous differences to confirm that the difference density obtained identified the selenomethionine sites (Fig. S4 and Table S2). *Bt* TubR*C*24 crystals were of space group C2, each asymmetric unit containing eight *Bt* TubR dimers and four *tubC*24 oligonucleotides. Electron density was surprisingly good (Fig. S4) and the positions after rigid body refinement resulted in close contacts but few clashes, implying a reasonable model; however, determination of the register of the DNA sequence lay beyond the resolution of our data.

***Bt* TubR*C* Crystals Contain a DNA–Protein Filament.** *Bt* TubR*C*24 forms an extended DNA–protein filament in our crystals. The DNA component, *tubC*24, describes a continuous linear fiber, curving in a slight right-handed superhelix, which forms the core of the complex. The outside of the filament is decorated with TubR molecules, forming an 8/1 helix with a rise of 38.4 Å, corresponding exactly to the 12-bp cognate repeat found in *Bt tubC* (Fig. 2 *C* and *D*). The coating of the outside of the DNA helix by *Bt* TubR enables the majority of crystal contacts to be formed between protein side chains rather than by DNA, as is expected because of the highly charged nature of the phosphate backbone. The *Bt* TubR*C*24 filament has very similar dimensions to the extended filaments observed by electron microscopy, and we conclude that this structure is representative of the predominant state of *Bt* TubR*C* in solution.

DNA Binding by *Bt* TubR. *Bt* TubR bound predominantly within the major groove of *tubC*. The N termini of the paired "recognition" helices together protrude deep into the major groove where they are able to make contact with 5 bp. This is the only major groove contact made, and it is therefore likely to correspond to the sequence-specific component of *Bt tubC*. The consensus binding sequence GTTTAA is not a simple twofold however, suggesting that DNA conformation must also play a role. On either side of the major groove binding site, the phosphate backbone descends into a cleft between the short helix and loop N-terminal to the recognition helix and the β-hairpin of *Bt* TubR. The negative charge of the phosphates will be complemented by lysines 43, 54, and 79, and arginine 74, which form the sides and base of this cleft. Finally, the tip of the β-hairpin protrudes toward the minor groove where arginine 77, which clashes with the phosphate backbone after rigid body refinement, must intrude into the groove itself (Fig. 2*E*).

Currently, only one other structure of a recognition helix dimerized form of the winged helix-turn-helix fold bound to DNA is available, that of FadR from *E. coli* (24). The DNA binding mode is conserved between the two structures, although the minor groove binding β-hairpin is positioned slightly differently in FadR. The conformation of the DNA in the two structures deviates substantially, however. Both proteins extend the DNA helix relative to its conformation in standard B-DNA; however in the case of FadR, the DNA is bound closely within the minor grooves, bending the course of the fiber toward the surface of the protein, whereas *Bt* TubR binds less closely in the minor groove, the DNA bending slightly away from the protein. The minor groove is also elongated, possibly due to the interaction with the β-hairpin. The full length of DNA contacted by a single *Bt* TubR dimer is 16 bp,

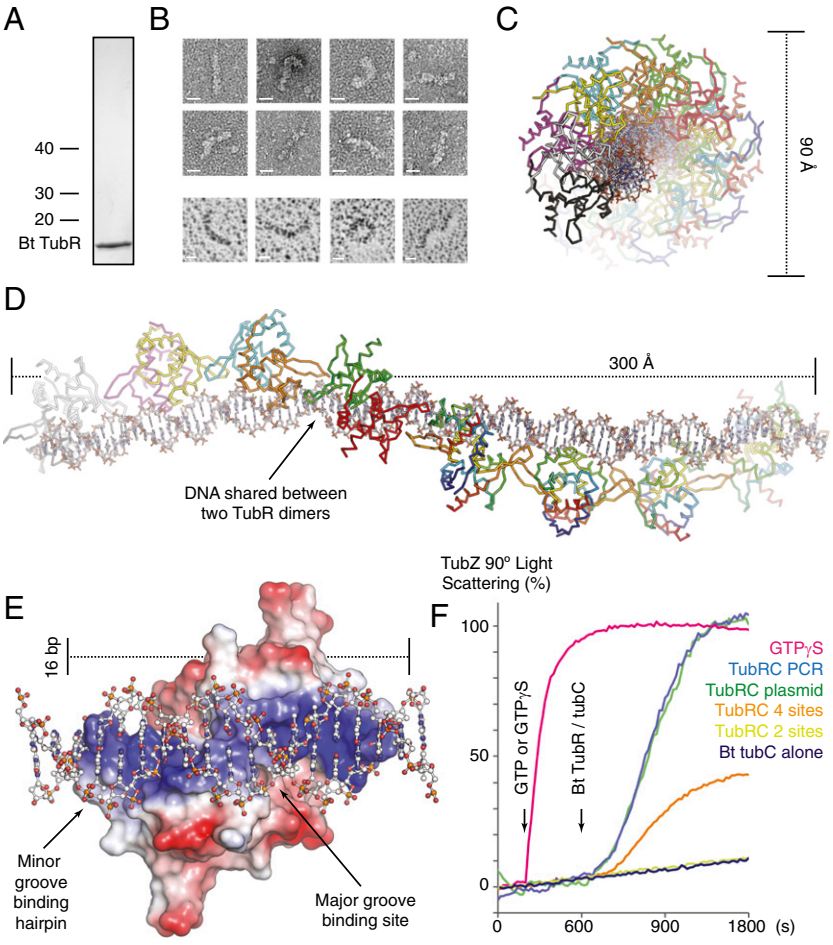

Fig. 2. *Bt* TubR bound to *tubC* forms a DNA–protein filament that effects TubZ polymerization. (*A*) Coomassie-stained SDS/PAGE of purified *Bt* TubR. (*B*) Electron micrographs of negatively stained (*Left*) and rotary shadowed (*Right*) *Bt* TubR bound to full-length *tubC* showing the morphology of the DNA–protein filaments formed. (Scale bars, 10 nm.) (*C* and *D*) Crystal structure of *Bt* TubR (Cα ribbon representation, the first four dimers are colored by chain, the second four a continuum between blue at the N terminus and red at the C terminus) bound to two repeats of *tubC* (stick representation, C in white/CPK colors). Dimensions in angstroms are shown alongside the structure, whereas the filament has been rotated by 90° between the two plates. (*E*) Single *Bt* TubR dimer (surface charge representation, red negative, blue positive) from the structure, with B-DNA [ball and stick representation, C in white/Corey, Pauling, Koltun (CPK) coloring] extended from the 12-bp section used in refinement in order to show the interaction with the full 16-bp region covered by the dimer. (*F*) Effect of *Bt* TubRC on the polymerization of TubZ measured using 90° light scattering. GTP or GTPγS was added to all reactions at 200 s, and the complexes indicated to the *Right* of the graph were added at 600 s (color coded). The four- and two-site versions of *Bt tubC* encompassed binding sites 4–7 and 6–7.

although the *tubC* repeat length is 12 bp (13). This requires 4 bp to be shared between adjacent dimers, which occurs at the site of protein–protein contact between the minor groove binding hairpins (Fig. 2 *C*–*E*). These β-hairpins from adjacent *Bt* TubR dimers are tightly paired in the minor groove, their opposition favoring the DNA curvature in the *Bt* TubR*C*24 structure.

TubRC Stabilizes TubZ Polymerization in Vitro. To confirm that the TubR*C* complex we had discovered was relevant to the activity of the TubZR*C* plasmid partitioning system, we assayed its effect on TubZ polymerization by 90° light scattering. A recent study by Oliva and colleagues (25) has shown that TubR*C* increases polymerization of TubZ. We therefore mixed *Bt* TubZ with GTP below the critical point of filament formation measurable by light scattering. *Bt* TubR*C* complex was then added, which stabilized filament growth. A similar effect, with the same maximum polymerization, can be produced by replacing GTP with GTPγS, implying that the bar to growth is due to hydrolysis of the nucleotide and disassembly of the filament at a higher rate than growth (Fig. 2*F*). Given that the *Bt* TubR*C* complex was present at a substoichiometric level, this suggests that it might prevent depolymerization of TubZ filaments, possibly switching from treadmilling to elongation.

To determine whether or not the whole *Bt* TubR*C* complex is required for the action of the system, we performed the assay with *Bt tubC* containing plasmid and with linear DNA representing full-length *tubC*, four repeats (sites 4–7) and two repeats (sites 6 and 7). These *Bt* TubR*C* complexes were compared at a constant concentration of TubR binding sites. *Bt* TubR*C* complexes bearing only two repeats did not have any measurable effect on TubZ polymerization below stoichiometric levels, whereas both linear DNA and plasmid containing *Bt tubC* showed a similar substoichiometric effect. The four-repeat long *Bt* TubR*C* complex affected polymerization; however, this effect was substantially reduced relative to full-length *tubC*, requiring four times as much complex to match polymerization (Fig. 2*F*).

TubR from a *tubZR* Operon in pBM400. Having defined *tubC* in the *Bt* TubZR*C* plasmid partitioning system and shown that *Bt* TubR*C* forms a flexible DNA–protein filament, the full length of which is required to match native in vitro efficacy, we moved on to consider whether or not there might be a preferred structural mode that the TubR*C* complex might take up, given that the flexible TubR*C* complex must presumably become ordered upon binding to the TubZ filament, which might explain the requirement for the length of *tubC*.

Fortuitously, in the course of our investigation of TubZR*C* plasmid partitioning systems we discovered an additional TubR homolog that adopts a more consistent preferred conformation as a DNA–protein complex, shedding light on this question. *Bm* TubR (UniProt Q848W2_BACMQ) lies within an operon containing a TubZ homolog in *B. megaterium* QM B1551 (*Bm*) plasmid pBM400 (Fig. S5). The gene encoding this TubR was synthesized and we overexpressed and purified the full-length protein without any tags or additions (Fig. 3*A*).

***Bm* TubR Forms Ring-Like DNA–Protein Filaments.** To determine whether or not the *Bm* and *Bt* TubR–DNA complexes were comparable, we imaged the *Bm* TubR–DNA complex by electron microscopy. Whereas *Bm* TubR binds its intergenic DNA 5′ to *tubZR* with a slight preference over *Bt tubC* (Fig. S3), we were unable to identify the exact *Bm* TubR binding sites by microarray (its structure suggests an explanation for this). Electron microscopy of *Bm* TubR bound to DNA revealed DNA–protein

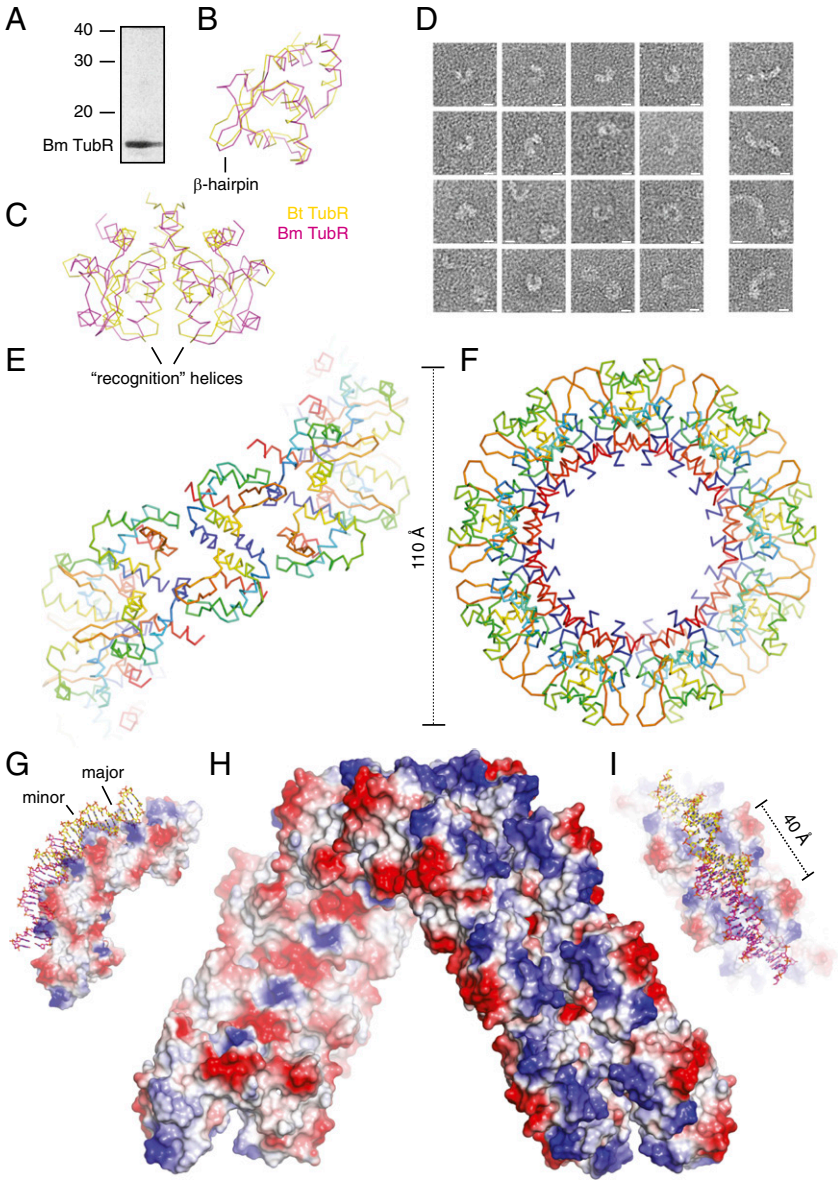

Fig. 3. *Bm* TubR forms helices of similar appearance in crystals and bound to DNA. (*A*) Coomassie-stained SDS/PAGE of purified *Bm* TubR. (*B*) Structural superimposition of monomers of *Bt* and *Bm* TubR (Cα ribbon representation, colored as indicated). (*C*) Structural superimposition of dimers of *Bt* and *Bm* TubR (Cα ribbon representation, colored as indicated). (*D*) Electron micrographs of negatively stained *Bm* TubR bound to *Bt tubC* DNA. (Scale bars, 10 nm.) (*E* and *F*) Crystal structure of *Bm* TubR helix (Cα ribbon representation, continuum between blue at the N terminus and red at the C terminus). Dimensions in angstroms are shown alongside the structure, whereas the helix has been rotated by 90° between the two plates. (*G*–*I*) Four *Bm* TubR dimers (surface charge representation, red negative, blue positive) with the DNA from Protein Data Bank (PDB) ID code 1HW2 (stick representation, C in yellow or magenta/CPK colors) shown after the two structures have been superimposed for the two central dimers. The two plates are rotated by 90° relative to one another. (*H*) Surface charge representation of the *Bm* TubR helix (red negative, blue positive).

filaments (Fig. 3*D*), the dimensions of which were similar to those recorded for *Bt* TubR*C* (*Bm* TubR formed identical DNA–protein filaments on intergenic, *Bt tubC*, and bulk DNA; *tubC* DNA was used here to allow direct comparison). The *Bm* TubR–DNA filament width averaged between 5 and 6 nm, and in general the filaments seemed similar in structure. In a notable contrast to the lack of a consistent preferred curvature by the *Bt* TubR*C* complex, however, although *Bm* TubR–DNA still produced relatively flexible filaments, they more often favored highly curved ring-like structures, with a typical diameter of 15–20 nm, mean 17.5, $n = 43$ (Fig. 3*D*). *Bm* TubR–DNA filaments adopted ring-like structures (defined as less than 15 nm separation between the tips of each end of the filament) and poorly ordered filaments in a ratio of 73.6:26.4 ($n = 253$), in contrast to *Bt* TubR*C*, for which the ratio was 10.7:89.3 ($n = 242$).

***Bm* TubR Is Structurally Homologous to *Bt* TubR.** To aid our understanding of *Bm* TubR, we crystallized the protein and recorded diffraction to 3.5 Å. The crystal structure was then solved by selenomethionine single anomalous dispersion (SeMet SAD). *Bm* TubR crystallized in space group H32, the asymmetric unit containing three protein molecules (Table S2). *Bm* TubR shares the same fold as *Bt* TubR, with a single chain backbone rmsd of 2.0 Å (Fig. 3*B*). Furthermore the quaternary structure of *Bt* TubR (13), in which the dimer is formed by twofold rotation about the recognition helix, is also recapitulated (Fig. 3*C*). In *Bm* TubR, the two monomers making up the dimer are splayed slightly, relative to those in *Bt* TubR, leaving a cleft between the recognition helices. Although it appears likely that this fissure may close slightly during DNA binding, the cleft may explain the observed lack of a clearly defined binding sequence. Superimposition of the surface of *Bm* TubR onto our structure of *Bt* TubR*C* shows that this cleft opens directly beneath the major groove: contacts with the DNA bases can therefore be expected to be substantially reduced. This implies that less base specific, more conformation-dependent minor groove binding may be expected to dominate, and that the overall protein–DNA contact area would also be considerably smaller, suggesting that larger numbers of dimers would be required to associate cooperatively for stable binding, whereas our microarrays cannot accommodate more than two dimers (Fig. S6). The putative DNA binding surface identified for *Bt* TubR is also conserved between the two proteins, a cluster of lysine and arginine residues characterizing the same face of the dimer (Fig. 3*H*) (13). The minor groove binding β-hairpin in *Bm* TubR is in a different

conformation from that in *Bt* TubR; however, this region has higher B factors in both cases, and given that it is also slightly separated from the body of the protein, it may be flexible in vivo.

***Bm* TubR Helices Externalize the DNA Binding Site.** Importantly, the dimers within the crystal structure of *Bm* TubR form helical filaments (Fig. 3 *E* and *F*). The dimensions of these helices are similar to the *Bm* TubR–DNA rings visualized by electron microscopy, with a filament width of 48 Å and a maximum helical width of 155 Å. The helices place *Bm* TubR dimers back to back, allowing the wedge-shaped proteins to make significant contacts with one another. The mean buried interface between pairs of dimers is 399.5 Å^2 in our structure of *Bt* TubR*C*, but this increases to 723.8 Å^2 in the case of our structure of *Bm* TubR. The extended β-hairpins of adjacent dimers are paired with a small gap between each dimer, extending the groove between recognition helices around the entire helix. Significantly this superstructure displays the positively charged DNA binding surface on the exterior of these helices (Fig. 3*H*).

Discussion

***Bm* TubR Helices Are in Principle Compatible with DNA Wrapping.** The length of DNA used to produce the ring-shaped *Bm* TubR–DNA filaments resolved by electron microscopy is consistent with DNA wrapping on the external surface. Ring diameter averaged 17.5 nm, implying a circumference of 55 nm, whereas the expected length of the PCR product would be 50 nm. The internal circumference would therefore be too short, whereas the external diameter would roughly match the expected length. Given the similarity in the dimensions of the *Bm* TubR–DNA rings, and the crystallographic helix, the most parsimonious explanation is that these structures are similar. If we assume that the DNA binding mode of *Bm* TubR is identical to that of *Bt* TubR, given their structural similarity, then superimposing the available structures of this class of DNA binding proteins (*Bt* TubR*C*/FadR–DNA) onto the structure of the *Bm* TubR helix will describe the path of the DNA. When this is carried out, it is clear that, although the surface is not immediately compatible with a continuous strand of DNA, only a relatively small distance (6.1 Å, *Bt* TubR*C*/3.4 Å, FadR–DNA) would separate the DNA backbones from adjacent dimers. FadR–DNA better matches the curve of the *Bm* TubR helix as the DNA from this structure curves in the same direction. Closer pairing of the minor groove binding β-hairpins would be required to bind DNA, which might be achieved through closure of the notch in the surface of *Bm* TubR or a slight rotation of the helix (Fig. 3 *G*–*I* and Fig. S7).

TubR*C* Is a DNA–Protein Filament. Our results conclusively show that the centromeric complex of TubZR*C* plasmid partitioning systems forms a DNA–protein filament. The disposition of *tubC* has evolved to facilitate its formation, ensuring coverage of a minimum length of plasmid DNA; furthermore, the binding mechanism of TubR is highly cooperative, allowing coating, further favoring its formation. We have shown that such a filament is required for the activity of TubR upon TubZ polymerization in vitro, activity falling to nil as the length of the centromeric complex decreases, even though the total concentration of TubR–DNA binding pairs was held constant. It is clear, therefore, that a TubR*C* filament is essential for the activity of the centromeric complex. Why must this be the case?

Interaction with the centromeric complex must stabilize the assembly of its cognate filament, whereas the free adapter protein must be incapable of this activity. The formation of the complex must therefore either produce a novel binding site between its components with substantially higher affinity or cluster the adapter protein in space to achieve binding to the filament through higher avidity. In both the ParMR*C* and TubZR*C* plasmid partitioning systems, it would seem that the second mechanism appears to have won out over the first. This may well occur because this mechanism can take advantage of both the clustering of the adapter protein on an array of DNA binding sites and clustering of the subunits within the cognate protein filament. Because the superstructure of a linear filament of identical subunits consists of a repeated vector, it must form a helix of tighter or looser curvature. Close clustering in space by a linear filament will therefore, by definition, be achieved through the formation of tight helical structures.

Although different TubZR*C* systems have so far been observed to have considerable similarity (25, 26), our *Bt* and *Bm* TubR complexes exhibit different curvatures. *Bt* TubR*C* crystallized as an extended DNA–protein filament with protein wrapping helically around the outside of the DNA, whereas the *Bm* TubR–DNA complex appears to form a ring or short helix with external DNA. Whereas it is possible that the two TubR*C* structures represent entirely diverged forms of the adapter complex, we think this unlikely; the *Bt* TubR*C* filament was clearly quite flexible in vitro, and it is in fact possible to reconcile the two structures as "flexible" and "curled" modes of a similar complex. The 12-bp repeat between major groove binding sites in the *Bt* TubR*C* filament is approximately conserved when DNA is superimposed upon the *Bm* TubR helix, so the binding periodicity would be similar (11–13 bp). The main structural change in DNA binding between the two would be rearrangement of the minor groove binding β-hairpins. These are roughly paired in both structures; however, the difference being that their orientation is reversed, providing a convenient switch between the two states. This proposed closure would neatly wrap the DNA and close up the space between adjacent TubR dimers (Fig. 4 *A* and *B* and Fig. S7).

Why then would the two DNA–protein filaments have different curvatures in vitro? One possible cause could be that binding

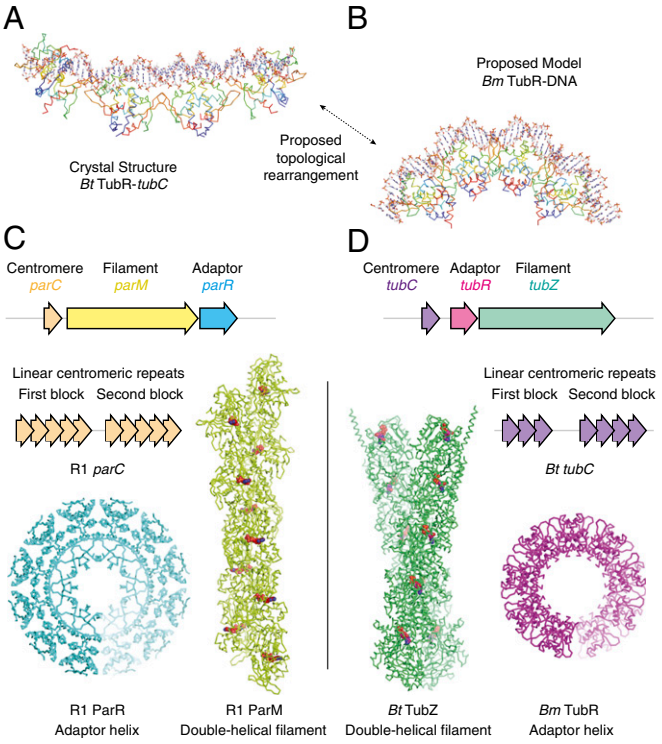

Fig. 4. *Bm* TubR helix suggests further convergent evolution of type II and III partitioning systems. (*A*) Structure of *Bt* TubR (Cα ribbon representation, blue at N terminus, red at C terminus) bound to *tubC* (stick representation, C in white/CPK colors). (*B*) Structure of *Bm* TubR (Cα ribbon representation, blue at N terminus, red at C terminus) shown with the DNA (stick representation, C in white/CPK colors) from PDB ID code 1HW2 after superimposition of the protein chains. (*C* and *D*) Comparison of operon structure (3, 10, 12), centromeric structure (20, 21), filament superstructure (9, 14, 16), and adapter complex superstructure (18, 19, this study) for the (actin-like) ParMR*C* and (tubulin-like) TubZR*C* plasmid partitioning systems.

to the TubZ filament is required to stabilize the TubR*C* complex in one state or another. It seems quite plausible that interactions with the linear filament stabilize the relatively flexible structure of the TubR*C* centromeric complex. The internally clustered TubR dimers in a ring-like structure would seem more capable of making a protein–protein contact than the sparsely distributed dimers in the flexible, extended form, as this form does not present TubR on a consistent side of the filament. The internal diameter of the *Bm* TubR crystal structure, at ~6.5 nm, is smaller than the diameter of the TubZ filament (14), at ~10 nm; however, the rings observed by electron microscopy exhibit internal diameters between 5 and 10 nm, allowing sufficient flexibility to encompass TubZ filaments in theory. A switch between a flexible and a ring-like form might allow the TubR*C* complex to clamp onto a growing TubZ filament during partitioning. Further structural studies of the TubZR*C* system will be required to understand the mechanism of binding and it is worth mentioning that the interaction sites between TubZ and TubR currently remain unknown.

Convergent Evolution of Type II and III Centromeric Complexes? It has not escaped our notice that an intriguing parallel emerges from this work. The structure of *Bt tubC* is strongly reminiscent of that of R1 *parC*, both consisting of two series of linear repeats separated by a linker, whereas the ring-like structure of *Bm* TubR is similar in superstructure to the known ParR*C* complex (Fig. 4*C*). This similarity adds to our earlier finding that TubZ, being tubulin related, forms actin- (and ParM)-like double helical filaments that are the smallest closed-symmetrical polymers possible and seem exquisitely tailored to the plasmid segregation task at hand (14). The observation of such similar superstructures, produced to perform similar functions by entirely unrelated proteins in different systems, suggests that convergent evolution may have taken place, driving both systems toward the same solution to the problem of binding a cytomotive filament, with entirely different protein and DNA building blocks.

Materials and Methods

Detailed information is provided in *SI Materials and Methods*. Briefly, all proteins were produced in *E. coli* and purified by chromatography; DNA was either synthesized (*Bt tubC*24), produced by PCR (all other linear DNA), or purified as a plasmid (p*tubC*); the *Bt tubC* aptamer microarray experiment was performed in conjunction with LC Sciences; electron microscopy was carried out using a 2% (wt/vol) uranyl acetate negative stain in an FEI T12 electron microscope; the sequence of *Bt tubC*24 was TTTAAGTTTAACTTTCAGTTTACA; *Bt* TubRC24 crystals were solved at 7 Å by molecular replacement and confirmed by selenomethionine SAD, whereas *Bm* TubR crystals were solved at 3.5 Å by selenomethionine SAD; 90° light scattering was carried out at 400 nm using 1.25 μM *Bt* TubZ, 500 nM TubR, and 125 nM of TubR binding sites in each *tubC* DNA, except for *tubC* repeats 4–7, where the concentration was doubled to make the difference from *tubC*24 clearly visible.

ACKNOWLEDGMENTS. We thank Rachel Larsen, Joseph Pogliano (both University of California at San Diego), and Katherine Michie [Medical Research Council Laboratory of Molecular Biology (MRC-LMB)] for providing materials; Sebastian Eustermann (MRC-LMB) for his tetraloop sequence; Fabrice Gorrec and Sonja Kuhlman for their help at MRC-LMB crystallization facility; Chen Shaoxia, Qing Wang, and Colin Palmer for their aid with electron microscopy at MRC-LMB; Sonja Dunbar for summer work and Ramona Duman (both MRC-LMB) for help at the European Synchrotron Radiation Facility (ESRF); and LC Sciences, the ESRF, and Diamond Light Source for their excellent service and support. This work was supported by Medical Research Council Grant U105184326.

1. Gerdes K, Howard M, Szardenings F (2010) Pushing and pulling in prokaryotic DNA segregation. *Cell* 141:927–942.
2. Salje J (2010) Plasmid segregation: How to survive as an extra piece of DNA. *Crit Rev Biochem Mol Biol* 45:296–317.
3. Gerdes K, Møller-Jensen J, Bugge Jensen R (2000) Plasmid and chromosome partitioning: Surprises from phylogeny. *Mol Microbiol* 37:455–466.
4. Austin S, Abeles A (1983) Partition of unit-copy miniplasmids to daughter cells. II. The partition region of miniplasmid P1 encodes an essential protein and a centromere-like site at which it acts. *J Mol Biol* 169:373–387.
5. Ogura T, Hiraga S (1983) Partition mechanism of F plasmid: Two plasmid gene-encoded products and a cis-acting region are involved in partition. *Cell* 32:351–360.
6. Leonard TA, Butler PJ, Löwe J (2005) Bacterial chromosome segregation: Structure and DNA binding of the Soj dimer—a conserved biological switch. *EMBO J* 24: 270–282.
7. Barillà D, Carmelo E, Hayes F (2007) The tail of the ParG DNA segregation protein remodels ParF polymers and enhances ATP hydrolysis via an arginine finger-like motif. *Proc Natl Acad Sci USA* 104:1811–1816.
8. Gerdes K, Larsen JE, Molin S (1985) Stable inheritance of plasmid R1 requires two different loci. *J Bacteriol* 161:292–298.
9. van den Ent F, Møller-Jensen J, Amos LA, Gerdes K, Löwe J (2002) F-actin-like filaments formed by plasmid segregation protein ParM. *EMBO J* 21:6935–6943.
10. Tang M, Bideshi DK, Park HW, Federici BA (2006) Minireplicon from pBtoxis of *Bacillus thuringiensis subsp. israelensis*. *Appl Environ Microbiol* 72:6948–6954.
11. Tinsley E, Khan SA (2006) A novel FtsZ-like protein is involved in replication of the anthrax toxin-encoding pXO1 plasmid in *Bacillus anthracis*. *J Bacteriol* 188:2829–2835.
12. Larsen RA, et al. (2007) Treadmilling of a prokaryotic tubulin-like protein, TubZ, required for plasmid stability in *Bacillus thuringiensis*. *Genes Dev* 21:1340–1352.
13. Ni L, Xu W, Kumaraswami M, Schumacher MA (2010) Plasmid protein TubR uses a distinct mode of HTH-DNA binding and recruits the prokaryotic tubulin homolog TubZ to effect DNA partition. *Proc Natl Acad Sci USA* 107:11763–11768.
14. Aylett CHS, Wang Q, Michie KA, Amos LA, Löwe J (2010) Filament structure of bacterial tubulin homologue TubZ. *Proc Natl Acad Sci USA* 107:19766–19771.
15. Hui MP, et al. (2010) ParA2, a *Vibrio cholerae* chromosome partitioning protein, forms left-handed helical filaments on DNA. *Proc Natl Acad Sci USA* 107:4590–4595.
16. Orlova A, et al. (2007) The structure of bacterial ParM filaments. *Nat Struct Mol Biol* 14:921–926.
17. Schumacher MA, Funnell BE (2005) Structures of ParB bound to DNA reveal mechanism of partition complex formation. *Nature* 438:516–519.
18. Møller-Jensen J, Ringgaard S, Mercogliano CP, Gerdes K, Löwe J (2007) Structural analysis of the ParR/*parC* plasmid partition complex. *EMBO J* 26:4413–4422.
19. Schumacher MA, et al. (2007) Segrosome structure revealed by a complex of ParR with centromere DNA. *Nature* 450:1268–1271.
20. Dam M, Gerdes K (1994) Partitioning of plasmid R1. Ten direct repeats flanking the parA promoter constitute a centromere-like partition site *parC*, that expresses incompatibility. *J Mol Biol* 236:1289–1298.
21. Tang M, Bideshi DK, Park HW, Federici BA (2007) Iteron-binding ORF157 and FtsZ-like ORF156 proteins encoded by pBtoxis play a role in its replication in *Bacillus thuringiensis subsp. israelensis*. *J Bacteriol* 189:8053–8058.
22. Eustermann S, et al. (2011) The DNA-binding domain of human PARP-1 interacts with DNA single-strand breaks as a monomer through its second zinc finger. *J Mol Biol* 407: 149–170.
23. Salje J, Löwe J (2008) Bacterial actin: Architecture of the ParMRC plasmid DNA partitioning complex. *EMBO J* 27:2230–2238.
24. Xu Y, Heath RJ, Li Z, Rock CO, White SW (2001) The FadR.DNA complex. Transcriptional control of fatty acid metabolism in Escherichia coli. *J Biol Chem* 276: 17373–17379.
25. Oliva MA, Martin-Galiano AJ, Sakaguchi Y, Andreu JM (2012) Tubulin homolog TubZ in a phage-encoded partition system. *Proc Natl Acad Sci USA* 109:7711–7716.
26. Chen Y, Erickson HP (2008) In vitro assembly studies of FtsZ/tubulin-like proteins (TubZ) from Bacillus plasmids: Evidence for a capping mechanism. *J Biol Chem* 283: 8102–8109.

Supporting Information

Aylett and Löwe 10.1073/pnas.1210899109

SI Materials and Methods

Sources. Unless stated, chromatography equipment was provided by GE Healthcare, chemicals by Sigma Aldrich, oligonucleotides by IDT, crystallography consumables by Hampton Research, and molecular graphics generated using PyMol (Schrödinger).

DNA, Genes, and Vectors. The genes encoding *Bacillus thuringiensis* serovar *israelensis* (ATCC; 35646) pBtoxis TubR and TubZ (UniProt Q8KNP2 and -3) were cloned directly from the species' DNA, kindly provided by R. A. Larsen and J. Pogliano (University of California, San Diego). The gene encoding *Bacillus megaterium* (ATCC 12872) pBM400 TubR (UniProt Q848W2) was synthesized, codon optimized (GenScript). Both expression vectors were based upon pHis17 (1). Construct pHis17–*Bt-tubR* encoded the complete sequence of *Bt* TubR and construct pHis17–*Bm-tubR* encoded the complete codon optimized sequence of *Bm* TubR. Constructs pHis17–*Bt-tubR*–His_6 and pET28–*Bt-tubZ*–His_6, adding six histidine residues at the C termini were also generated. These constructs were used solely for the microarray and light scattering experiments; no changes were made to the published sequence of either protein. The DNA sequence for *Bt tubC*24 was TTTAAGTTTAACTTTCAGTTTACA and its complement. Full-length *Bt tubC* was represented by a PCR product encompassing base pairs 126510–126649 of pBtoxis, repeats 1–3 by 126607–126654, and repeats 4–7 by 126526–126573, whereas the pBM400 intergenic region was represented by 44230–44369. Plasmid p*tubC* consisted of full-length *Bt tubC* product cloned into pHis17.

DNA Microarray. A DNA microarray was produced that consisted of 24-bp double-stranded variable sequences as 60-bp hairpins capped using a tetraloop sequence and scanned through the region of pBtoxis between base pairs 122000 and 3100 by 4-bp increments, and the region around *tubZR* (between base pairs 126787 and 126451) by 1-bp increments. This experiment was carried out through the aptamer microarray service at LC Sciences, Houston. Briefly, 0.2 μg/mL *Bt* TubR–His_6 was applied to the microarray in 100 mM Tris·Cl 8.5, 100 mM NaCl, 1 mM EDTA, 1% (wt/vol) BSA at 30 °C for 2 h. The chip was then washed with the same buffer without protein, and Alexa-647 labeled antihexahistidine antibody applied to the chip in the same fashion as protein for 1 h. The chip was washed once more and then scanned at 635 nm. The discrete Fourier coefficient for each whole number of base pairs was calculated and subsequently plotted against the base pair repeat as shown in Fig. S1.

Electrophoretic Mobility Shift Assays. The indicated PCR products were produced from primers 5′ conjugated to fluorescein. DNA was purified by gel extraction and then incubated with the indicated concentrations of *Bt* or *Bm* TubR in a final volume of 10 μL standard TBE buffer supplemented with 0.1 mg/mL BSA and 5% (vol/vol) glycerol for 30 min at 25 °C. Protein–DNA complexes were separated by native PAGE using Criterion 4–20% TBE gels according to the manufacturer's instructions (BioRad). The fluorescein-labeled DNA was detected using a Typhoon Trio imager (GE Healthcare) using the manufacturer's recommended standard sensitivity settings for fluorescein.

Light Scattering (90°). Light scattering experiments were performed using a Perkin-Elmer LS55 luminescence spectrometer in 25 mM Tris·Cl pH 8.0, 100 mM KCl, 2 mM $MgCl_2$, 0.5 mM EDTA at 20 °C with constant stirring of the 1-mL quartz cuvettete. Excitation and emission wavelengths were held at 400 nm, and the photon multiplier set to 650 V. TubZ was added to a final concentration of 1.25 μM, whereas 250 μM nucleotide was added at the indicated time point. *Bt* TubR was added to a final concentration of 500 nM when indicated, and the concentration of identified TubR binding sites within the DNA added was held constant at 125 nM, except in the case of *Bt tubC* with four TubR binding sites (sites 4–7), where this concentration was doubled to allow the effect upon polymerization to be clearly visible for the benefit of the reader.

Electron Microscopy. *Bt* or *Bm* TubR (10 mg/mL) and 100 μM of a 150-bp PCR product containing *Bt tubC* or the *Bm* intergenic region were diluted 2,000-fold into 25 mM Na-Hepes pH 7.5, 50 mM KCl, 1 mM $MgCl_2$. Samples were applied to carbon-coated Cu/Rh 300 mesh grids (Agar Scientific). The grids were blotted and stained with 0.5% (wt/vol) uranyl formate. Images were recorded to film (Kodak Electron; 1 s) or CCD (TVIPS; F214) using a Tecnai T12 electron microscope (FEI) at 120 kV, −2 to −6 μm defocus.

Rotary Shadowing. Before shadowing, *Bt* TubR*C* was diluted into 100 mM ammonium hydrogencarbonate, 50% (vol/vol) glycerol, giving a final concentration of 0.1 mg/mL. The sample was applied to carbon-coated grids, dried under high vacuum for 4 h, and then shadowed. Rotary shadowing was performed with an Edwards E306A coating system using a molten platinum source at an oblique angle of 3° and at a sample-to-source distance of 10 cm.

Protein Expression. C41 *E. coli* (Invitrogen) carrying the requisite expression vector were grown in 12 L 2xYT broth or M9 media, for selenomethionine (Acros Organics) substituted protein, according to the protocol of van den Ent and colleagues (2). Cultures were supplemented with 100 μg/L ampicillin or 50 μg/L kanamycin as appropriate and grown at 37 °C. Expression was induced by addition of isopropyl-β-D-1-thiogalactopyranoside to a final concentration of 1 mM, at an optical density at 600 nm of 1.0, and cells were harvested by centrifugation at 4 × *g* after 18 h expression at 20 °C.

Protein Purification. The pellet yielded by 1 L bacterial culture was resuspended in 20 mL 100 mM Na-Hepes pH 7.0 and broken at 25 kpsi, 4 °C using a cell disruption system (Constant Systems). Protein was then purified by chromatography from the supernatant after centrifugation at 45,000 × *g*. TubR proteins were retrieved by heparin affinity chromatography (5 mL HiTrap heparin HP, 25 mM Na-Hepes pH 7.0, 0–1 M NaCl), followed by purification by ion exchange (5 mL HiTrap Q HP, 25 mM Tris·Cl pH 8.5, 0.1–0.5 M NaCl) and size exclusion chromatography (HiLoad Sephacryl S200 16/60, 25 mM Tris·Cl pH 8.5, 0.1 M NaCl, 1 mM EDTA, 1 mM NaN_3). Protein was concentrated to 10 mg/mL before and after size exclusion chromatography in 20 mL, 10-kDa cutoff centrifugal concentrators (Vivaspin). TubZ protein was retrieved by nickel affinity chromatography (HisTrap HP, Tris·Cl pH 8.5, 0–1 M imidazole gradient), and crystallographic purity achieved by ion exchange (HiTrap Q HP, Tris·Cl pH 8.5, 100–500 mM NaCl gradient) followed by size exclusion chromatography (HiLoad Sephacryl S200 16/60, Tris·Cl pH 8.5, 150 mM NaCl, 1mM EDTA, 1mM NaN_3).

Crystallization. Initial conditions were identified using the high-throughput Medical Research Council Laboratory of Molecular Biology (MRC-LMB) crystallization facility (3). *Bt* TubR–*tubC* crystals were produced in 500 nL to 500 nL protein to precipitant drops: 10 mg/mL *Bt* TubR, 500 μM *tubC*24 or -26, 100 mM Na-

Hepes pH 7.5, 5 mM $MgCl_2$, 25% (wt/vol) polyacrylic acid 5100 sodium salt. Artificial mother liquor supplemented to 25% (vol/vol) glycerol was used as a cryoprotectant. *Bm* TubR crystals were produced in 500 nL to 500 nL protein to precipitant sitting drops: 20 mg/mL *Bm* TubR, 100 mM Tris·Cl pH 8.5, 0.2 M sodium citrate, 15% (vol/vol) PEG 400. Artificial mother liquor supplemented to 30% (vol/vol) PEG 400 was used as a cryoprotectant.

Crystallography. Diffraction images of *Bm* TubR and *Bt* TubR–*tubC*24 crystals were collected at European Synchrotron Research Facility beamline ID29 and Diamond beamline I03. Diffraction images were processed with XDS (4), POINTLESS (5), and SCALA (6). Initial phases for *Bm* TubR were determined by single wavelength anomalous dispersion (SAD). The Se substructure was solved with SHELXCDE (7) and phases were calculated with PHASER (8). The model was built manually with MAIN (9) and refined with REFMAC5 (10) and PHENIX (11). Initial phases for both *Bt* TubR–*tubC* crystal structure were determined by molecular replacement using PHASER (8) with ideal B-form DNA from Web3DNA (12) and Protein Data Bank (PDB) ID code 3M8E as search models. The models were refined as rigid bodies using PHENIX, the DNA being split into 12-bp double-stranded sections to allow for distortion. Selenium SAD anomalous differences were reserved for validation, the calculated phases from refinement being used to phase the anomalous differences. Anomalous scattering peaks were visible at the sites occupied by the selenium atoms of the selenomethionine residues, validating the structure independently (Fig. S3).

Structural Calculations. Structural superimpositions and alignments were carried out using the DALI-lite webserver (13). The output *Z*-score for PDB ID codes 3M9A and 4ASN was 10.9 and the rmsd, 2.0 Å. Surface area calculations were performed using the PDBe-PISA webserver and PDB ID codes 4ASN and 4ASO (14).

1. Miroux B, Walker JE (1996) Over-production of proteins in *Escherichia coli*: Mutant hosts that allow synthesis of some membrane proteins and globular proteins at high levels. *J Mol Biol* 260:289–298.
2. van den Ent F, Lockhart A, Kendrick-Jones J, Löwe J (1999) Crystal structure of the N-terminal domain of MukB: A protein involved in chromosome partitioning. *Structure* 7:1181–1187.
3. Stock D, Perisic O, Löwe J (2005) Robotic nanolitre protein crystallisation at the MRC Laboratory of Molecular Biology. *Prog Biophys Mol Biol* 88:311–327.
4. Kabsch W (2010) XDS. *Acta Crystallogr D Biol Crystallogr* 66:125–132.
5. Evans P (2006) Scaling and assessment of data quality. *Acta Crystallogr D Biol Crystallogr* 62:72–82.
6. Collaborative Computational Project, Number 4 (1994) The CCP4 suite: Programs for protein crystallography. *Acta Crystallogr D Biol Crystallogr* 50:760–763.
7. Sheldrick GM (2008) A short history of SHELX. *Acta Crystallogr A* 64:112–122.
8. McCoy AJ, et al. (2007) Phaser crystallographic software. *J Appl Cryst* 40:658–674.
9. Turk D (1992) Weiterentwicklung eines Programms für Molekülgraphik und Elektronendichte-Manipulation und seine Anwendung auf verschiedene Protein Strukturaufklärungen [Improvement of a computer program for molecular graphics and electron density manipulations and its application for various protein structure determinations] (PhD thesis, Technical University of Munich, Germany).
10. Murshudov GN, Vagin AA, Dodson EJ (1997) Refinement of macromolecular structures by the maximum-likelihood method. *Acta Crystallogr D Biol Crystallogr* 53:240–255.
11. Adams PD, et al. (2010) PHENIX: A comprehensive Python-based system for macromolecular structure solution. *Acta Crystallogr D Biol Crystallogr* 66:213–221.
12. Zheng G, Lu X-J, Olson WK (2009) Web 3DNA—a web server for the analysis, reconstruction, and visualization of three-dimensional nucleic-acid structures. *Nucleic Acids Res* 37(Web Server issue):W240-6.
13. Holm L, Park J (2000) DaliLite workbench for protein structure comparison. *Bioinformatics* 16:566–567.
14. Krissinel E, Henrick K (2007) Inference of macromolecular assemblies from crystalline state. *J Mol Biol* 372:774–797.

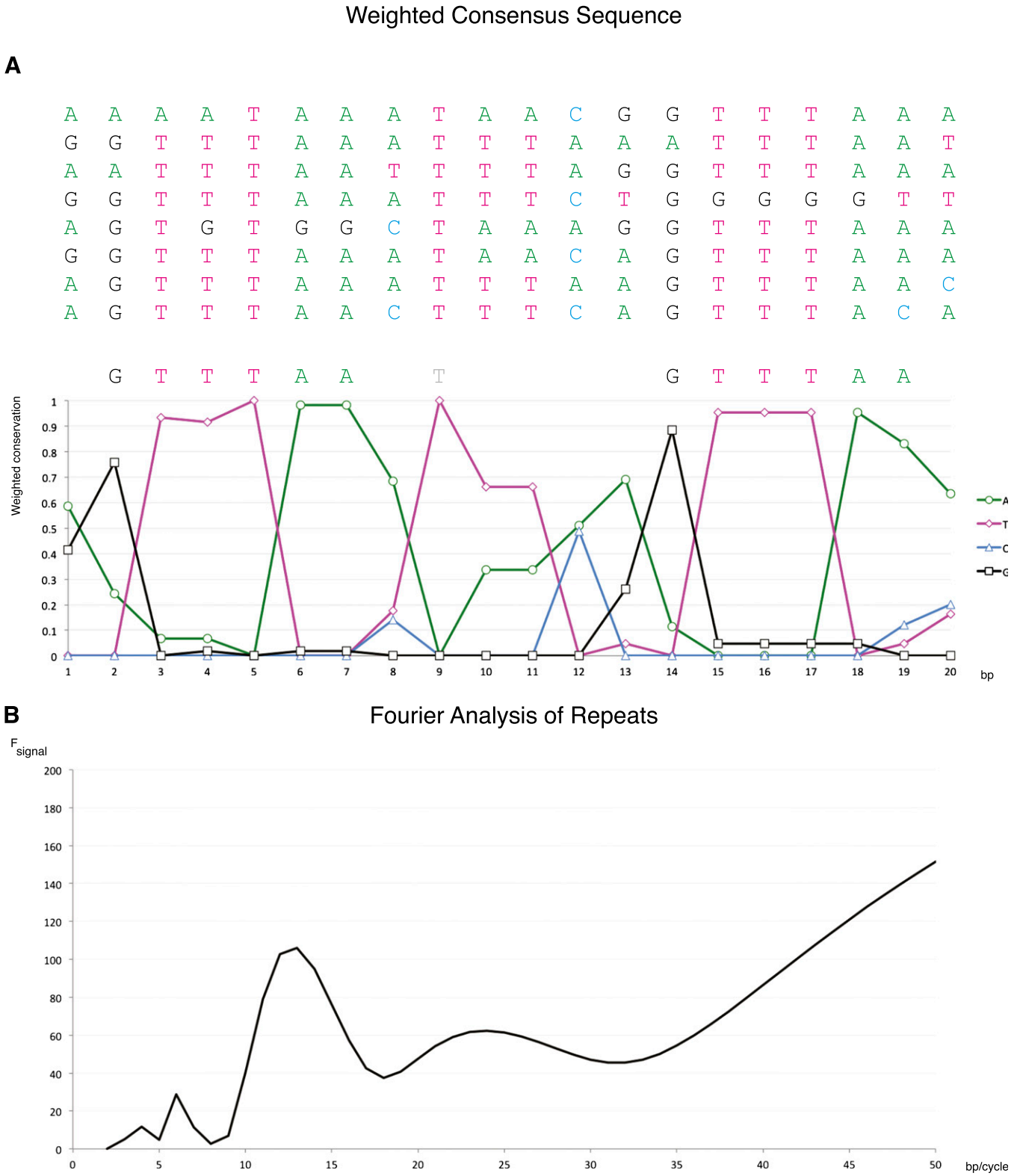

Fig. S1. Assignment of the repeat length and consensus sequence of *Bt* TubR binding sites in *tubC*. (*A*) Aligned sequences of the seven peaks of *Bt* TubR binding and graph of the weighted alignment below (total summing to unity). (*B*) Graph of Fourier magnitudes of *Bt* TubR binding signal against reciprocal base pair repeat, sites 4–7.

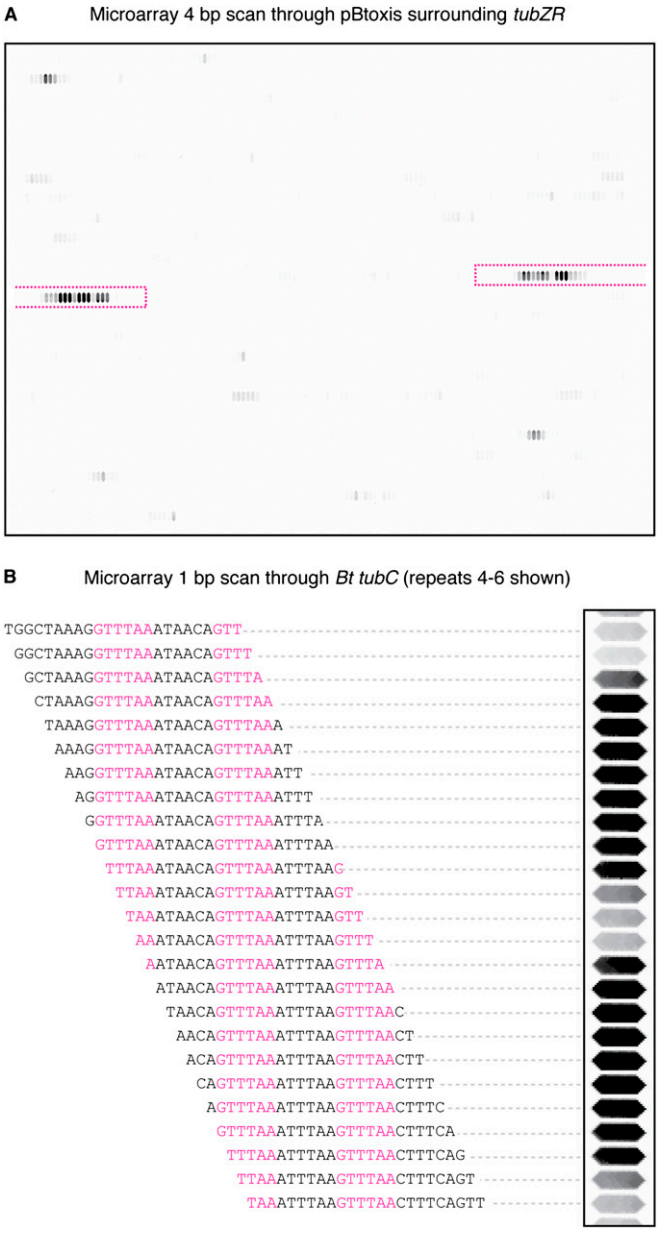

Fig. S2. A *Bt tubC* microarray was probed with TubR. (*A*) An area of the *Bt tubC* microarray showing binding of *Bt* TubR (black) to sequences sampled at 4-bp intervals through pBtoxis (bp 122000 to 3100). The sequence runs from left to right, top to bottom. (*B*) Part of the microarray showing binding of *Bt* TubR (black) to sequences sampled at 1-bp intervals through part of *Bt tubC* (bp 126577 to 126530), the aligned sequences of the hairpins are shown, magenta indicating the consensus site.

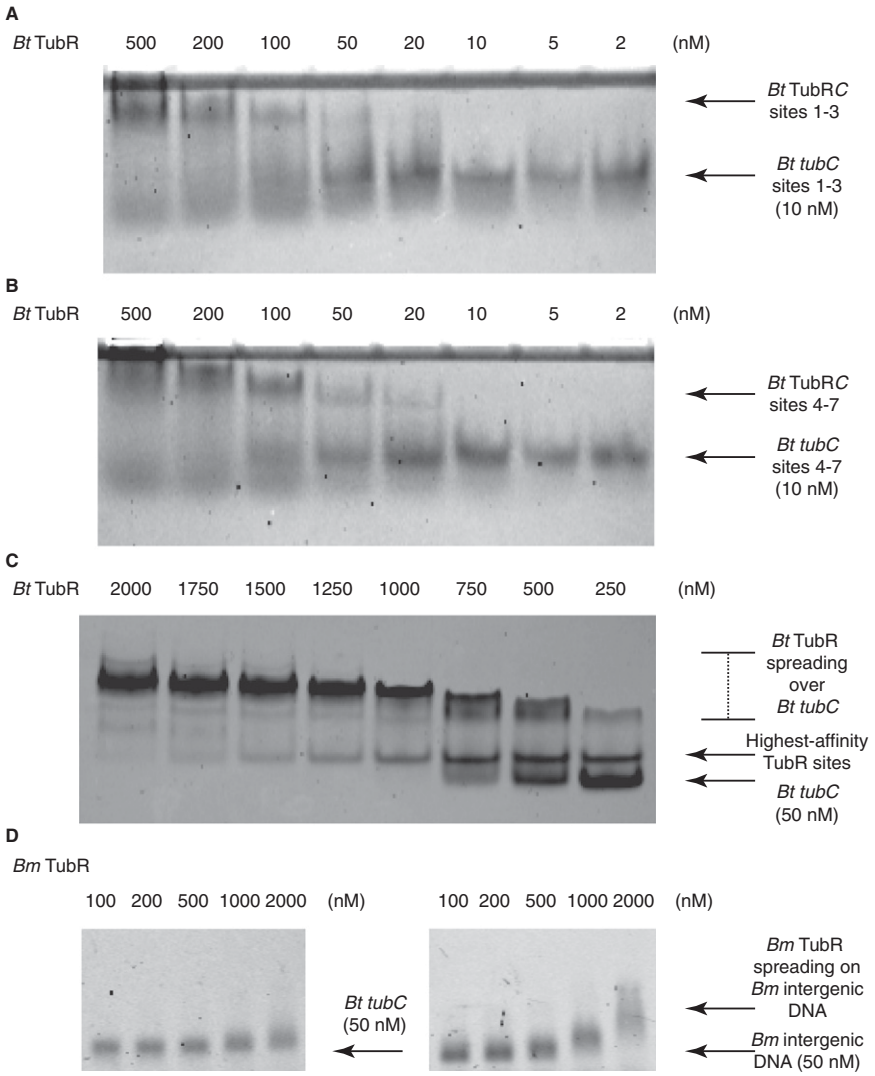

Fig. S3. *Bt* TubR binds cooperatively to both sets of *tubC* repeats. (*A*) Electrophoretic mobility shift assay showing binding by TubR during titration against repeats 1–3 of *tubC*. (*B*) Electrophoretic mobility shift assay showing binding by TubR during titration against repeats 4–7 of *tubC*. (*C*) Electrophoretic mobility shift assay showing binding by TubR during titration against full-length *tubC*. Initial binding to high-affinity sites is visible as a single band slightly above the initial DNA, and the gradual curve thereafter during titration implies lateral spreading by *Bt* TubR. (*D*) Electrophoretic mobility shift assay showing that *Bm* TubR shows a binding preference toward its 5′ intergenic DNA (*Right*), compared with *Bt tubC* DNA (*Left*). All scans show fluorescence from 5′ fluorescein conjugation.

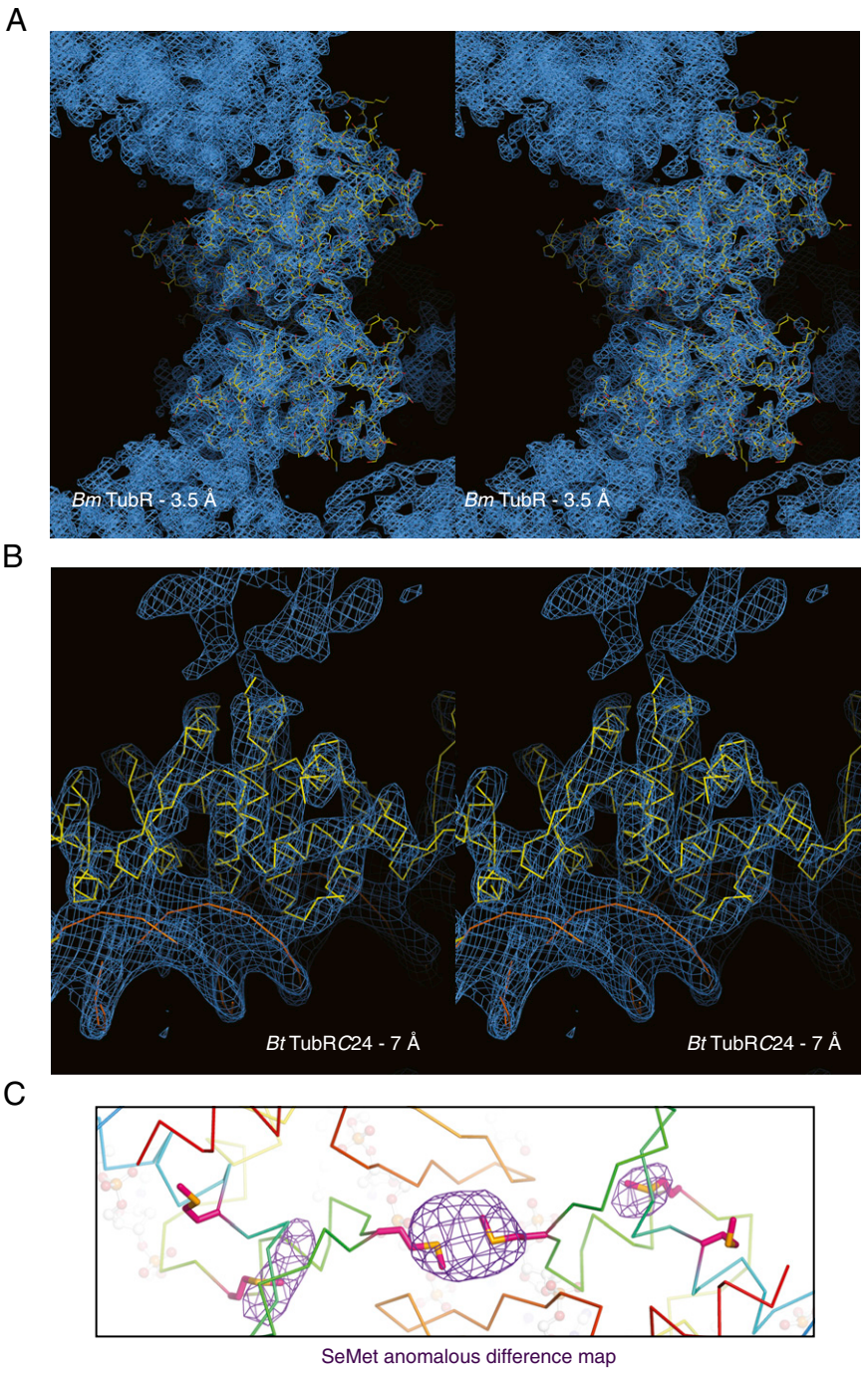

Fig. S4. Electron density from the crystal structures of TubR. (*A*) Stereoscopic images of the structure of *Bm* TubR (density at 1.5 σ in blue, stick representation, C in yellow/CPK colors). (*B*) Stereoscopic images of the structure of *Bt* TubRC24 (density at 1.5 σ in blue, Cα ribbon representation in yellow for protein and brown for DNA). (*C*) Region of the Se anomalous difference map from the structure of *Bt* TubRC24 at 3 σ (purple mesh), Cα ribbon representation, with selenomethionine residues highlighted [stick representation, C in magenta/Corey, Pauling, Koltun (CPK) colors].

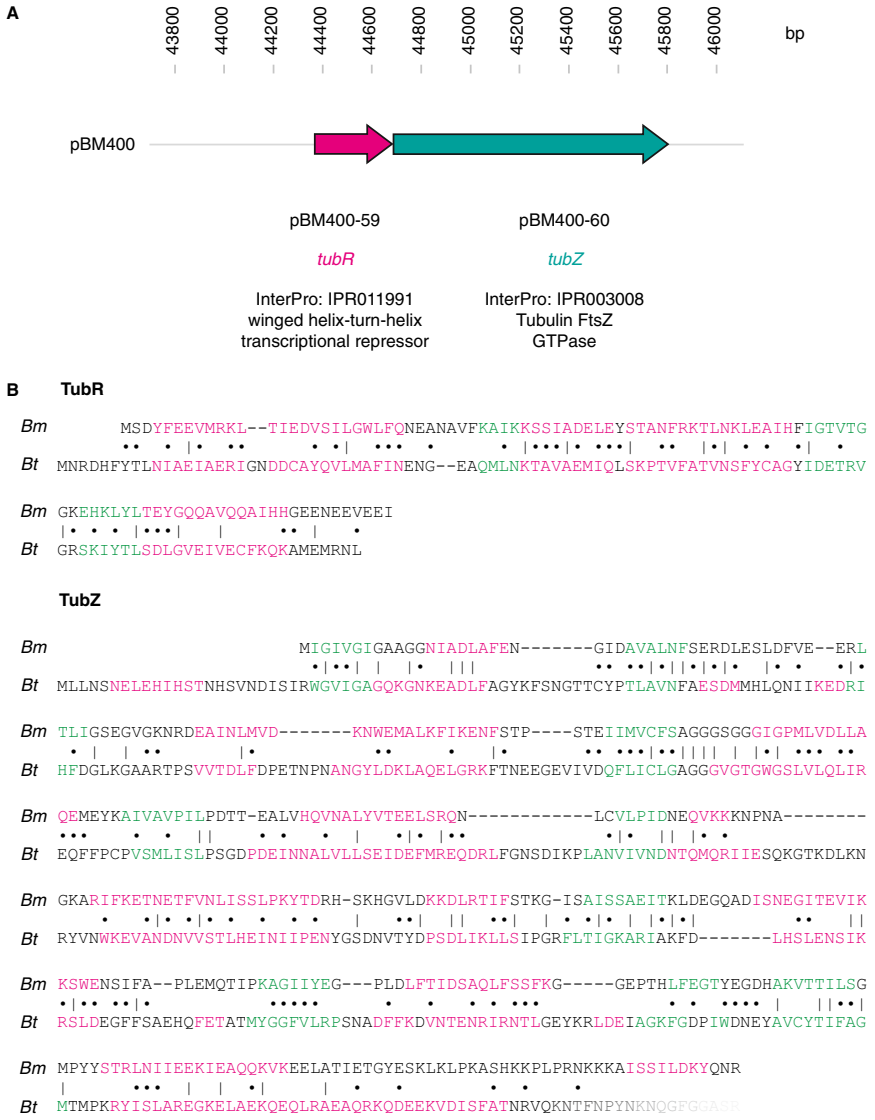

Fig. S5. The *tubZR* operon from *Bacillus megaterium* pBM400. (*A*) Schematic showing the genes *tubR* and *tubZ* in pBM400. InterPro family results (May 2012) are shown to confirm the identity of the two genes. (*B*) Protein sequence alignments of *Bm* TubR and TubZ with *Bt* TubR and TubZ.

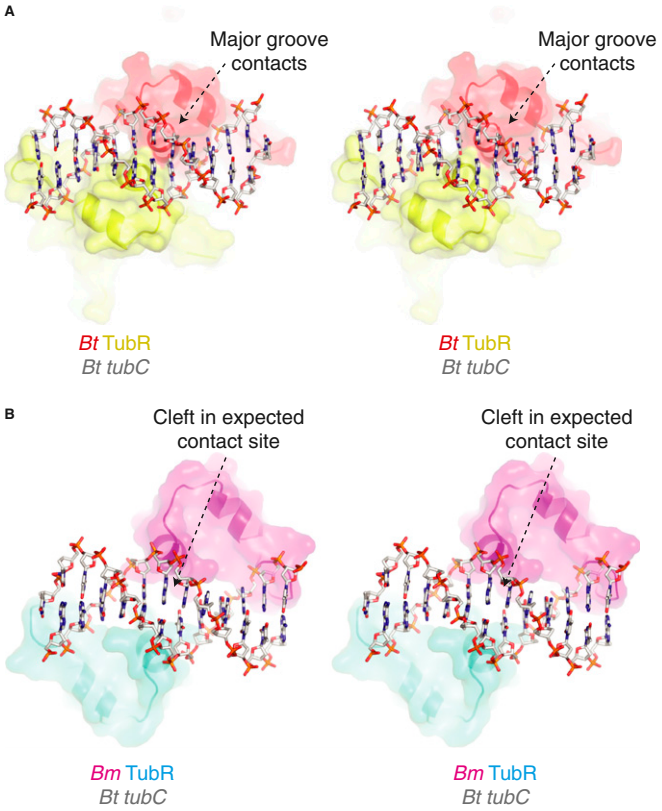

Fig. S6. Superimposition of a *Bm* TubR dimer onto the structure of *Bt* TubRC showing the reduced binding surface within the major groove. (*A*) Stereoscopic image of the structure of one dimer and DNA from *Bt* TubRC (red and yellow, surface representation on cartoon, DNA in CPK colors) showing the major groove contact surface against DNA. (*B*) Stereoscopic image of a structural superimposition of the structure of a *Bm* TubR dimer (cyan and magenta, surface representation on cartoon) onto the Bt TubRC filament (DNA shown only, white and CPK colors) showing the *predicted* major groove contact surface against DNA.

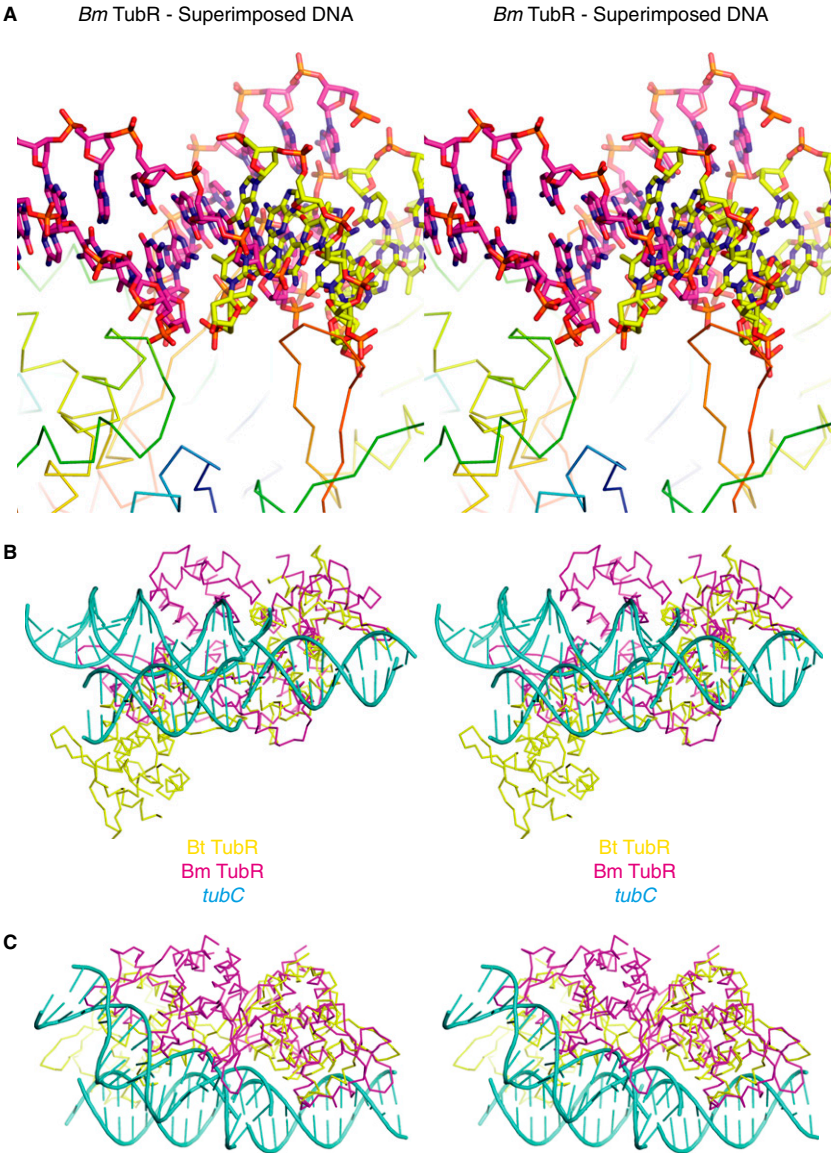

Fig. S7. Two possible modes of binding by TubR to *tubC*. (*A*) Stereoscopic images of the structure of *Bm* TubR (Cα ribbon representation, blue at N terminus, red at C terminus) with DNA (stick representation, C in yellow or magenta/CPK colors) from homologous structure PDB ID code 1HW2 shown after the protein chains have been superimposed. (*B* and *C*) Stereoscopic images of the superimposition of *Bt* TubRC24 (Cα ribbon representation, yellow) and *Bm* TubR (magenta). DNA is shown in cartoon representation, in blue. DNA in the *Bm* TubR form is from PDB ID code 1HW2.

Table S1. Previous experimental results from *Bt* TubR–DNA complexes

Publication	Reference	Experiment	Data/result	Conclusions
Tang et al. (2006)	(1)	Deletion map of this operon	Located *tubZRC* operon	Minireplicon locus (then proposed)
		Sequence analysis of locus	Four repeats (then identified)	*Cis*-acting site in locus DNA
		Gene deletion study	TubR and TubZ were required	Replication genes (then proposed)
Larsen et al. (2007)	(2)	Gene deletion study	TubZ increased if *tubR* deleted	TubR regulates this operon
		Plasmid stability assay	*tubZRC* required for plasmid stability	*tubZRC* plasmid partitioning system
Tang et al. (2007)	(3)	DNA deletion study	DNA repeats necessary	Replication origin (then proposed)
		EMSA of TubR and DNA repeats	TubR binds DNA repeats	TubR is an iteron binding protein
		EMSA of TubR/DNA and TubZ	TubR-DNA binds TubZ	TubR is a regulator of TubZ
Ni et al. (2010)	(4)	Crystallography of TubR in the absence of DNA	TubR structures without DNA at high resolution	Recognition helix dimer/possible DNA binding face
		Mutation of TubR surfaces	Impaired binding to DNA repeats	Dimerization and surfaces required
		Fluorescence polarization of TubR/DNA	TubR titrates to ~8 molecules before inflection	TubR binds ~1 dimer per 12 bp
		Fluorescence polarization of TubR/DNA against TubZ	TubR and DNA interacted with TubZ with H11, but not without	TubZ C terminus required for this interaction

1. Tang M, Bideshi DK, Park HW, Federici BA (2006) Minireplicon from pBtoxis of *Bacillus thuringiensis subsp. israelensis*. *Appl Environ Microbiol* 72:6948–6954.
2. Larsen RA, et al. (2007) Treadmilling of a prokaryotic tubulin-like protein, TubZ, required for plasmid stability in *Bacillus thuringiensis*. *Genes Dev* 21:1340–1352.
3. Tang M, Bideshi DK, Park HW, Federici BA (2007) Iteron-binding ORF157 and FtsZ-like ORF156 proteins encoded by pBtoxis play a role in its replication in *Bacillus thuringiensis subsp. israelensis*. *J Bacteriol* 189:8053–8058.
4. Ni L, Xu W, Kumaraswami M, Schumacher MA (2010) Plasmid protein TubR uses a distinct mode of HTH-DNA binding and recruits the prokaryotic tubulin homolog TubZ to effect DNA partition. *Proc Natl Acad Sci USA* 107:11763–11768.

Table S2. Crystallographic data summary

Statistics	*Bacillus megaterium* TubR	*Bacillus thuringiensis* TubR – *tubC*24
Protein	Full length, untagged	Full length, untagged
UniProt ID no.	Q848W2	Q8KNP2
ATCC ID no.	12872	35646
Collection		
Beamline	ESRF-ID29	Diamond-I03
Wavelength, Å	0.9790	0.9794
Crystal		
Space group	H 3 2	C 1 2 1
Cell, Å	179.9, 179.9, 114.3	519.3, 63.7, 167.3 β = 96.7
Scaling		
Resolution	3.5	7.0
Completeness (%)*	100 (100)	98.1 (98.5)
Multiplicity*	9.9 (10.4)	5.9 (5.9)
Ano completeness (%)*	99.3 (100)	98.1 (97.9)
Ano multiplicity*	4.9 (5.1)	3.2 (3.2)
Ano correlation*,†	0.658 (0.021)	0.858 (0.008)
(I)/σ(I)*,‡	23.1 (4.8)	10.9 (1.3)
R_{merge}*	0.053 (0.431)	0.090 (1.642)
R_{pim}*	0.026 (0.205)	0.052 (0.817)
Phasing		
Scatterer/mode	Se/SAD	Se/MR-SAD
Number of sites	3	
Figure of merit	0.72	
Refinement		
R/R_{free}§	0.1858/0.2284	0.3443/0.3712
Bond length rmsd, Å	0.013	
Bond angle rmsd, °	1.324	
Most favored, %**	86.3	
Disallowed, %**	0	
Deposition		
PDB ID code	4ASN	4ASO

*Values in parentheses refer to the highest recorded resolution shell.
†Anomalous correlation coefficient between half sets (SCALA).
‡Resolution cutoff determined by half-shell correlation coefficient falling below 0.7.
§5% of reflections were randomly selected before refinement.
**Percentage of residues in the Ramachandran plot (PROCHECK).